Clim Dyn (2017) 48:3741–3758
DOI 10.1007/s00382-016-3299-9

The impact of changes in parameterizations of surface drag and vertical diffusion on the large-scale circulation in the Community Atmosphere Model (CAM5)

Jenny Lindvall[1,2] · **Gunilla Svensson**[1,2] · **Rodrigo Caballero**[1,2]

Received: 5 April 2016 / Accepted: 25 July 2016 / Published online: 18 August 2016

Abstract Simulations with the Community Atmosphere Model version 5 (CAM5) are used to analyze the sensitivity of the large-scale circulation to changes in parameterizations of orographic surface drag and vertical diffusion. Many GCMs and NWP models use enhanced turbulent mixing in stable conditions to improve simulations, while CAM5 cuts off all turbulence at high stabilities and instead employs a strong orographic surface stress parameterization, known as turbulent mountain stress (TMS). TMS completely dominates the surface stress over land and reduces the near-surface wind speeds compared to simulations without TMS. It is found that TMS is generally beneficial for the large-scale circulation as it improves zonal wind speeds, Arctic sea level pressure and zonal anomalies of the 500-hPa stream function, compared to ERA-Interim. It also alleviates atmospheric blocking frequency biases in the Northern Hemisphere. Using a scheme that instead allows for a modest increase of turbulent diffusion at higher stabilities only in the planetary boundary layer (PBL) appears to in some aspects have a similar, although much smaller, beneficial effect as TMS. Enhanced mixing throughout the atmospheric column, however, degrades the CAM5 simulation. Evaluating the simulations in comparison with detailed measurements at two locations reveals that TMS is detrimental for the PBL at the flat grassland ARM Southern Great Plains site, giving too strong wind turning and too deep PBLs. At the Sodankylä forest site, the effect of TMS is smaller due to the larger local vegetation roughness. At both sites, all simulations substantially overestimate the boundary layer ageostrophic flow.

Keywords Orographic drag · Boundary layer · Climate model · Community atmosphere model · Turbulent mountain stress

1 Introduction

The drag on the atmospheric flow is of great importance for the circulation and climate in numerical weather prediction (NWP) and global climate models (GCMs). Changes in surface friction can, for example, result in shifts in the location of the storm tracks (Chen et al. 2007) and affect baroclinic cyclones (Adamson et al. 2006). Yet, it is not well known how vertical diffusion and orographic drag should be represented. There is a lack of understanding of some of the relevant atmospheric processes and it is still unclear how observations from point measurements should be translated into parameterized grid-box averages of turbulence and drag. The issue of both representing the large-scale circulation and the near-surface climate accurately and doing so for the right reasons has long been recognized as a challenge for GCMs and numerical weather prediction (NWP) models (Sandu et al. 2013; Holtslag et al. 2013).

The first Global Energy and Water Cycle Experiment (GEWEX) Atmospheric Boundary Layer Study (GABLS1, Cuxart et al. 2006), showed that the turbulence closures employed in operational models are more diffusive in stably stratified conditions than what is seen in large-eddy simulations (LES) and in observations. However, it can be claimed that the mixing in stable conditions needs to be enhanced in order to account for processes that contribute to the vertical mixing but are not represented in

✉ Jenny Lindvall
lindvall@misu.su.se

[1] Department of Meteorology, Bolin Centre for Climate Research, Stockholm University, Stockholm, Sweden

[2] Swedish e-Science Research Centre, Stockholm, Sweden

the models. Examples of such processes are unresolved surface heterogeneity, differential heating, certain sources of gravity waves and mesoscale variability. Mahrt (1987) argued that the area-averaged flux in an area might differ from the flux that would be due to the area-averaged variables since small subregions of strong mixing might exist in regions dominated by stable stratification. McCabe and Brown (2007) investigated the role of surface heterogeneity, by using area-averaging techniques on very high-resolution nighttime simulations to calculate effective stability functions. They only found justification for a significant enhancement of the stability functions below the height of 50 m.

One reason for having stronger mixing in stable conditions is to reduce or prevent a night-time cold bias and a decoupling from the surface by mixing down warmer air from above, while another is to decrease the synoptic activity in the model (Viterbo et al. 1999; Mauritsen 2012). With a higher diffusivity, the lifetime of synoptic cyclones appears to decrease. The increase in surface stress together with deeper boundary layers increases the vertically integrated cross-isobaric flow into a cyclone, thus affecting its development (Svensson and Holtslag 2009; Adamson et al. 2006; Beare 2007).

Too much diffusion, however, has long been known to be detrimental to simulations of the stable boundary layer. It has been documented, for example in GABLS1, that the wind turning in the boundary layer becomes too small, the planetary boundary layer height (PBLH) too high and low level jets tend to be smoothed out and located too far from the surface (Brown et al. 2005, 2008; Cuxart et al. 2006; Svensson and Holtslag 2009). The ECMWF model employs enhanced diffusion and Sandu et al. (2013) concluded that while reducing the diffusion improved the simulation of the stable boundary layer, the near-surface temperature and the large-scale circulation were degraded. Brown et al. (2008) reported an improvement in near-surface winds without a degradation of the large-scale circulation after reducing the diffusivity over sea in stable conditions and including a non-local momentum mixing in convection conditions in the UK Met Office Model.

The drag and mixing in the models are not only influenced by the turbulence parameterizations. Model developments include explicit treatments of the subgrid scale gravity waves (Palmer et al. 1986; McFarlane 1987). There are also parameterizations that take into account turbulence generated by subgrid-scale orography. A common approach is to use an effective roughness length, a concept developed by Fiedler and Panofsky (1972). They define the effective roughness length of an area with heterogeneous topography as the roughness length that the same area with homogeneous terrain would have to have to give the same surface stress. As global or even widespread observations of surface stress over land are lacking, the size of the effective roughness length becomes somewhat arbitrary. It is, however, used in many weather forecast models and GCMs. One of these is the Community Atmosphere Model version 5(CAM5, Richter et al. 2010; Neale et al. 2010),which we analyze in this study. More advanced approaches include parameterizations that allow for explicit treatment of low-level flow-blocking due to subgrid orography (Lott and Miller 1997; Gregory et al. 1998) and turbulent orographic form drag (Beljaars et al. 2004). Sandu et al. (2016) showed that the magnitude of orographic drag in a NWP model has a substantial impact on both 10 day weather forecasts and seasonal integrations during winter.

In this study, we analyze the effect of changes to the surface drag and the vertical diffusion in the atmospheric component (CAM5.3) of the Community Earth System Model (CESM) 1.2. Between the previous version the atmospheric component, CAM4, and the present, CAM5, large changes in the parameterization of turbulence were made. The changes included going from a more diffusive turbulence scheme to a more restrictive scheme with short-tail stability functions that shuts off all turbulence completely at high stabilities (Bretherton and Park 2009). As the change to a less diffusive scheme was done in CAM5, a turbulent mountain stress (TMS) parameterization that adds a strong orographic surface stress, based on an orographic roughness length approach, was instead included (Richter et al. 2010; Neale et al. 2010). Together with changes in many of the other parameterizations, the performance of the model was substantially improved (Hurrell et al. 2013; Kay et al. 2012). One improved feature was the blocking frequency, although it still presents a problem in some regions and seasons (R. Neale, personal communication). As blocking events affect the large-scale flow and can redirect migrating cyclones, they have a large impact on the weather and climatology of a region. It is therefore of interest to understand what causes the changes in blocking frequency.

TMS is known to have large effects on the surface winds (Lindvall et al. 2013) and therefore also on the circulation of the atmosphere. In this study, we document the effects of making changes to the atmospheric drag in CAM5 and we compare the default CAM5 with a simulation without orographic TMS. As enhanced diffusion is commonly used in large-scale models and is considered advantageous for the synoptic activity, we also compare with two versions that are more diffusive at high stabilities but are without the orographic surface stress of the TMS parameterization. This enables us to evaluate the differential impacts of orographic surface drag and more turbulent diffusion. The analysis is done both for large-scale features but also in comparison with detailed boundary layer observations at two locations.

Section 2 describes the experiment setup and the data used for evaluation. The results are presented in Sects. 3 and 4 gives a summary of the study.

2 Methods

2.1 Theory

Simulations with CESM1.2 and its atmospheric component CAM5.3 (Neale et al. 2010) are used to investigate the effect of the treatment of vertical diffusion and orographic drag. In the model physics, the turbulence, gravity wave and the shallow and deep convection parameterizations all exert drag on the atmosphere. A large part of the unresolved drag is represented in CAM5 by to the University of Washington moist turbulence scheme (Bretherton and Park 2009). It is sometimes referred to as a PBL scheme, although it allows for turbulence at all levels in the atmosphere. The scheme is a local, diagnostic turbulent kinetic energy (TKE) scheme, developed to improve stratus and stratocumulus topped boundary layers. Convective and stably stratified turbulent layers are diagnosed using the moist Richardson number and several decoupled layers may exist in an atmospheric column. Downgradient mixing is assumed to occur in all turbulent layers and the eddy diffusivity is calculated using the diagnostic TKE. TKE storage is neglected and, in stably stratified layers, the TKE transport is also assumed to be negligible. In the standard CAM5 physics, the turbulence closure constants result in a critical Ri of 0.19 (Fig. 1), above which all turbulence is cut off (i.e., short-tail stability functions).

In order to take into account the effect of unresolved orography, a turbulent mountain stress (TMS) parameterization is employed (Richter et al. 2010; Lindvall et al. 2013). The unresolved surface orographic drag is parameterized as a turbulent surface drag using an effective roughness length dependent on the standard deviation of the topographic height (σ) in the grid cell. It is scaled using a scaling factor (f(Ri)) based on the Richardson number (Ri) : $f(Ri) = 1$ if $Ri < 0, f(Ri) = 0$ if $Ri > 1$ and $f(Ri) = 1 - Ri$ if $0 \leq Ri \leq 1$. The orographic roughness length is defined $z_{0oro} = \min(0.075\sigma, 100)$. If the vegetation roughness length is small, this usually gives a very large effect of orographic drag even in regions with little topography. The vegetation roughness length of grassland is 0.06 m in CESM which would require a σ of only 0.8 m over an entire grid box to get the same z_{0oro}. For example, even at the flat, grassland ARM site at the Southern Great Plains, σ is 18.5 m, which gives a z_{0oro} of 1.4 m, substantially larger than 0.06 m.

Gravity wave drag for stationary waves generated by subgrid scale orography is parameterized following McFarlane (1987). The magnitude of the stress is given by a source function that depends on the height of the orography, the Brunt–Väisällä frequency and the wind speed in the source region. The deep convection scheme is developed by Zhang and McFarlane (1995) and modified to include convective momentum transports (Richter and Rasch 2008) and a modified dilute plume calculation (Neale et al. 2008). Shallow convection is parameterized using the University of Washington shallow cumulus scheme (Park and Bretherton 2009), developed to work tightly together with the moist turbulence scheme. The scheme combines a mass-flux closure with a trigger based on convective inhibition. The convection parameterizations remove very little kinetic energy from the atmosphere compared both to the turbulence scheme and to the gravity wave drag. However, the convection parameterizations are important in order to redistribute momentum in the atmosphere through vertical transport.

2.2 Model simulations

The simulations are ten year long AMIP-type runs with CAM5.3 using climatological sea surface temperatures for the period 1982–2001 (Hurrell et al. 2008). The horizontal resolution is 0.9° latitude × 1.25° longitude and the model has 30 vertical levels. Although CESM is normally run with prognostic aerosols, all simulations discussed here use a prescribed aerosol distribution (corresponding to the year 2000), in order to remove the influence of near-surface wind speeds on aerosol loading and thus on climate.

The configurations of all simulations are summarized in Table 1. Four main simulations are analyzed. The control simulation (CTRL) uses the default CAM5.3 physics. In NoTMS, the turbulent mountain stress parameterization is turned off. Longtail is also run without TMS, but with the stability function in the turbulence scheme replaced with a longer tail function (see Fig. 1), retaining turbulence at larger Richardson numbers. In order to focus on the effect of a long tail, the stability functions are only changed for higher stabilities. For the near-neutral and weakly stable cases they are the same as in the default CAM5 (Fig. 1). Finally, PBL Longtail is the same as Longtail, but with the stability functions replaced only within the boundary layer. However, the longer tail stability functions still have rather small values at high stabilities, compared to many other operational models. For comparison, the revised Louis functions, used by the IFS model at the European Centre for Medium-Range Weather Forecasts (ECMWF, Sandu et al. 2013), are included in Fig. 1. The stability functions in CTRL and in the two Longtail simulations are the same for near-neutral and unstable Richardson numbers. In the two Longtail simulations, there is also a small background diffusion, approximately equivalent to the molecular diffusion of air.

Table 1 A summary of the simulations analyzed in this study. See text for further details

Simulation name	TMS	Comment
CTRL	Yes	
NoTMS	No	
Longtail	No	The short-tail stability function in the turbulence scheme is replaced with a longer tail function. Background diffusion is included
PBL Longtail	No	The short-tail stability function in the turbulence scheme is replaced with a longer tail function, but only in the PBL. Background diffusion is included
TMStopo	Yes	TMS is only applied where the height of subgrid orography >100 m
GWNoTMS	No	The speeds of the source winds for the gravity wave parameterization are halved
TMSv2	Yes	TMS is always on and does not depend on Ri

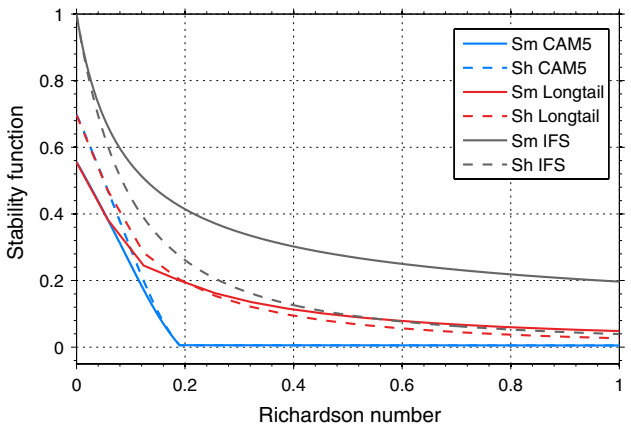

Fig. 1 Turbulence closure stability functions in stably stratified conditions for heat (*dashed lines*) and momentum (*solid lines*) in default CAM5.3 (*blue*, Bretherton and Park 2009), the Longtail simulation (*red*) and IFS (*grey*, Sandu et al. 2013)

In addition to the three main simulations, three complementary experiments are carried out to analyze the effects on the blocking frequency.

2.3 Observational and reanalysis data

The simulated atmospheric blocking frequency is evaluated against two reanalyses, ERA-interim (Simmons et al. 2007) and the Modern Era Retrospective-Analysis for Research and Applications (MERRA, Rienecker et al. 2011). Daily values of the 500-hPa geopotential height are used for the time period 1979–2012.

The model simulations are also compared to boundary layer observations at two well-established measurement sites for atmospheric research. One is the Atmospheric Radiation Measurement (ARM) site at the Southern Great Plains in Oklahoma, US The site is dominated by grassland, located at 97.5°W, 36.6°N and situated 318 m above sea level. The best estimate dataset (ARMBE, Xie et al. 2010) provides radiosonde data of wind and temperature with approximately 6-hourly intervals as well as surface turbulent heat fluxes. The friction velocity, used in calculations of the boundary layer height, is from the Ameriflux network dataset (Fischer et al. 2007), which overlaps with the ARMBE dataset for the period 2002–2007. The other site is Sodankylä, a boreal forest site in northern Finland (26.6°E, 67.4°N, 179 m above sea level). Seven years of Sodankylä soundings data and turbulent surface fluxes are provided by the Coordinated Energy and Water Cycle Observation Project (CEOP) archived by the NCAR Earth Observing Laboratory (EOL; http://data.eol.ucar.edu) and by CarboEurope (http://www.carboeurope.org).

2.4 Blocking definition

We define atmospheric blockings following Barriopedro et al. (2006), and their adapted version of the Tibaldi and Molteni (1990) index. Tibaldi and Molteni (1990) defined blockings using the 500-hPa height difference in the storm track regions. The geopotential height gradients north (GHGN) and south (GHGS) are computed for each longitude point:

$$GHGN = \frac{Z(\lambda,\phi_N) - Z(\lambda,\phi_0)}{\phi_N - \phi_0} \quad (1)$$

$$GHGS = \frac{Z(\lambda,\phi_0) - Z(\lambda,\phi_S)}{\phi_0 - \phi_S} \quad (2)$$

$$\phi_N = 80°\mathrm{N} + \Delta, \phi_0 = 60°\mathrm{N} + \Delta, \phi_S = 40°\mathrm{N} + \Delta, \quad (3)$$

where $Z(\lambda,\phi)$ is the 500-hPa geopotential height at latitude ϕ and longitude λ. For Δ, we use all latitude points $\pm 5°$. A longitude is considered blocked if these constraints are fulfilled for at least one value of Δ:

$$\begin{aligned} GHGN &< -10\,\mathrm{gmp}\,{}^{\circ}\mathrm{lat}^{-1} \\ GHGS &> 0 \end{aligned} \quad (4)$$

The 500-hPa geopotential height anomaly at ϕ_0 is also required to be positive, a constraint proposed by Barriopedro

et al. (2006) to prevent the diagnosis of cutoff lows as blockings. The blocking extent is required to be at least 12.5° in longitude, allowing 2.5° of those to be unblocked. A minimum duration of five days is required for the blockings, allowing one unblocked day between two blocked. To consider a blocking continuously present, at least one of the blocked longitudes must remain so the following day.

The last ten years in ERA-Interim and MERRA do not reveal any major differences compared to the 34-year mean blocking frequency (not shown), indicating that the ten year simulations are long enough to study blockings.

2.5 Cross-isobaric flow

Synoptic systems and the large-scale circulation are affected by boundary-layer wind turning, which gives the ageostrophic flow in the boundary layer (Adamson et al. 2006; Beare 2007; Svensson and Holtslag 2009). The strength of the ageostrophic flow can be estimated following Svensson and Holtslag (2009). The planetary boundary-layer momentum equations for the mean flow are derived from the Navier-Stokes equations by neglecting molecular viscosity and horizontal turbulent momentum flux divergence and introducing Reynolds averaging to separate the mean and the turbulent part of the flow (e.g. Stull 1988; Holton and Hakim 2012). Assuming further a stationary and horizontally homogeneous flow, the ageostrophic wind is a function only of the vertical stress divergence in the direction of the geostrophic wind:

$$f\overline{v} = \frac{\partial \overline{u'w'}}{\partial z}, \tag{5}$$

where f is the Coriolis parameter, $\overline{v}$ is the mean ageostrophic wind and $\overline{u'w'}$ is the vertical momentum flux in the direction of the geostrophic wind. Neglecting the turbulent momentum flux above the boundary layer, where it is generally small, and vertically integrating to the top of the boundary layer results in:

$$f\int_0^h \overline{v}dz \approx -\overline{u'w'}_0 = u_*^2 \cos\alpha, \tag{6}$$

where u_* is the friction velocity and α the angle between the surface stress and the geostrophic wind. Thus, the right hand side can be seen as an estimate of the cross-isobaric flow or as the cross-isobaric mass flux when multiplied by the density.

3 Results

The climate in the simulations is similar in CTRL and NoTMS when it comes to the radiative fluxes at the top of the atmosphere. The net radiative flux at the top of the atmosphere is 5.2, 5.2 and 4.9 W m^{-2} in CTRL, PBL Longtail and NoTMS, respectively. Longtail differs slightly from these two with a value of 7.3 W m^{-2} and the discrepancy appears to be mainly due to differences in the longwave radiative flux. The values in all simulations are larger than what is observed and larger than the value in the default CAM5 (Zhao et al. 2013), possibly because of our use of prescribed aerosols (valid for the year 2000) instead of the regular prognostic aerosol scheme.

Figure 2a–d shows the total stress magnitude, which over land is much larger in CTRL than in the other simulations because of TMS. In the CTRL simulation, TMS dominates completely over all land regions, but especially in mountain areas where the magnitude of the TMS is one order of magnitude larger than the sum of the other contributions to the surface stress. Disregarding TMS, by far the largest contribution to the surface drag is due to vertical diffusion. Figure 2b–d can therefore be regarded as an approximation of the stress from the turbulence scheme for the NoTMS and Longtail simulations. Gravity waves only affect the surface stress in high-topography regions (Fig. 2e–h), while the deep and shallow convection parameterizations only redistribute momentum.

For comparison, Fig. 2i shows the magnitude of the surface stress for the CTRL simulation with the TMS contribution subtracted. It is apparent that the other parameterizations partially compensate for the absence of TMS in NoTMS and the Longtail simulations. TMS reduces the surface winds substantially and therefore acts to decrease the stress from both turbulence (compare Fig. 2i with Fig. 2b–d) and gravity waves over land (Fig. 2a–h). However, despite a slight compensation, the total surface stress is much larger in CTRL (Fig. 2a–d) over land.

Figure 2k–n shows the bias in the wind stress over ocean compared to the ERS scatterometer (Stoffelen and Anderson 1997a, b). CTRL and NoTMS are fairly similar over the oceans, as TMS only acts over land. All simulations overestimate the stress in the Southern Hemisphere storm track region and over the North Atlantic, but the bias in CTRL is smaller over the Atlantic. The Longtail simulation has a far too strong surface stress in the storm track regions in both hemispheres. Longtail and PBL Longtail have more diffusion in stable situations. In Longtail, this does not only increase the boundary-layer drag, but since the free troposphere is mostly stably stratified it also increases the vertical diffusion at higher levels, especially in the jet regions. The net result is seen as an increase in the surface stress, especially in the storm track regions. The effect of enhanced diffusion only in the PBL has a minor impact on the surface stress over oceans (compare Fig. 2l, n). This is most likely because the stability functions are not changed for weakly stable boundary layers (see Fig. 1) and ocean

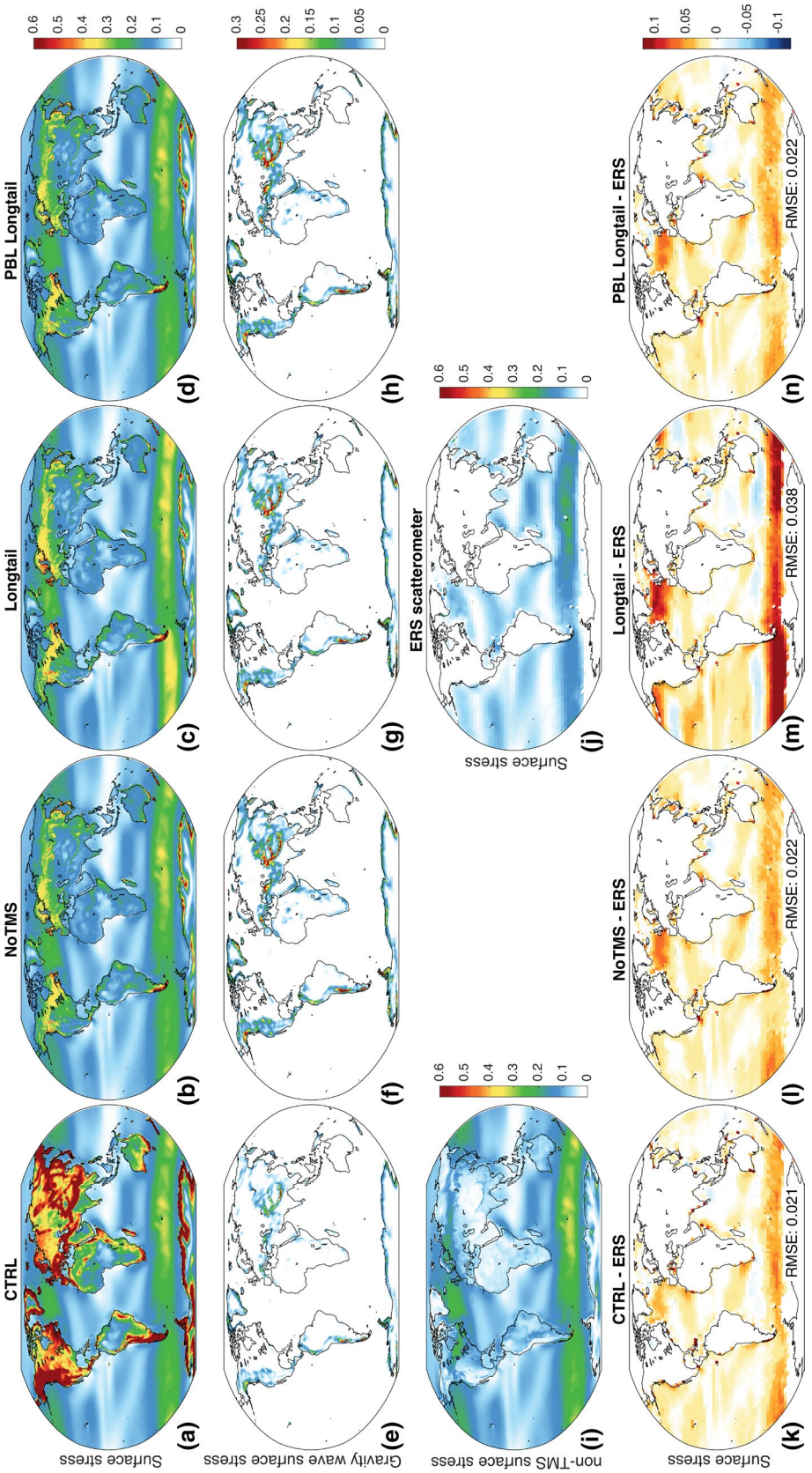

Fig. 2 Annual mean surface stress magnitude $|\tau| = \sqrt{\tau_x^2 + \tau_y^2}$ (N m^{-2}). **a–d** Shows the total surface stress magnitude, **e–h** the magnitude of the gravity wave surface stress and **i** the magnitude of total surface stress except for TMS in CTRL. **j** The observed surface wind stress over ocean from the ERS scatterometer and **k–n** The bias in magnitude and direction of the surface wind stress over ocean. The magnitude of surface stress in **j–n** is calculated using monthly means of zonal and meridional surface stresses. RMSE values are area averaged over ocean regions only. Note that scales vary for the different surface stresses. Please also note that highest values of the total surface stress magnitude (**a–d**) lies outside the plotted range. CTRL extends all the way up to 19.9 N m^{-2} and the other three simulations have maximum values of 0.9–1.2 N m^{-2}

boundary layers are seldom very stably stratified (Garratt 1992).

It is obvious in Fig. 2 that the surface drag is very different in CTRL and Longtail compared to NoTMS and PBL Longtail and this also has an effect on the model circulation. One notable difference is in the position and strength of the Icelandic and Aleutian lows. The largest model discrepancies are found in spring and therefore Fig. 3 shows the mean sea level pressure in March–May. The CTRL simulation agrees quite well with ERA-Interim (Simmons et al. 2007), while the sea level pressure is much lower over the Arctic in the simulations without orographic surface stress compared to both CTRL and ERA-Interim. In NoTMS the difference compared to ERA-Interim is as large as −12 hPa with a RMSE of 5.7 hPa (Fig. 3c). Enhancing the diffusion throughout the atmosphere as in Longtail degrades the simulation rendering a RMSE of 8.7 hPa (Fig. 3d). However, when only increasing the diffusion in the boundary layer the simulation is improved, although PBL Longtail is still not as good as CTRL with subgrid orographic drag (Fig. 3b, e). It does seem as if the orographic drag and the boundary layer diffusion have similar effects on the circulation in this aspect.

The seasonal mean zonal anomaly of the 500-hPa stream function in the Northern Hemisphere is shown in Fig. 4 for ERA-Interim and the four model simulations. There are substantial differences in all seasons, both between the models and ERA-Interim and between the different model simulations. The differences appear, however, to be larger in the transition seasons than in winter and summer. Generally, CTRL and PBL Longtail are the simulations that closest agree with ERA-Interim, while Longtail exhibits large discrepancies. The large inter-model differences in the 500-hPa stream function anomaly and in the Icelandic low indicate that the changes made in the parameterizations of drag has a substantial impact on the large-scale circulation.

Figure 5 shows that the zonal wind is too strong in all simulations in both hemispheres. In CTRL the subgrid-scale orographic stress appears to give an improvement in the Northern Hemisphere throughout the atmospheric column, but it does not have an effect on the bias in the Southern Hemisphere, which is as large as in NoTMS. Enhancing the diffusion, which is common practice in many climate models and leads to an increase in the surface drag and an increase in cross-isobaric flow (Svensson and Holtslag 2009) should give weaker zonal winds. However, having the longer tail stability functions in the PBL Longtail does not alleviate the biases (Fig. 5e), possibly because of the very moderate long tail. Using the longtail functions throughout the atmosphere even degrades the simulation and gives a dipole bias in the midlatitudes, implying a poleward-shifted jet (Fig. 5d). In the idealized study by Chen et al. (2007), an increase in surface friction weakened and shifted the jet equatorward. It is therefore apparent that the enhanced diffusion in Longtail does not have the same effect as an increase in surface friction. However, the result of a stronger jet being shifted poleward is in agreement with Chen et al. (2007).

Figure 6 shows the annual mean 2-m temperature in the CRU observational data set (Mitchell and Jones 2005) and the difference between the model simulations and the CRU data. It is clear that despite the apparent differences in the large-scale circulation, CTRL, NoTMS and PBL Longtail have similar near-surface temperature climates. NoTMS and PBL Longtail are slightly closer to what is observed and have a smaller warm bias over the central North America than CTRL. Replacing the short-tail with a longer-tail stability function throughout the atmosphere severely degrades the simulation by amplifying the warm bias in the Northern Hemisphere midlatitudes. However, such a comparison might not be entirely fair, considering that the model has been tuned for the CTRL settings. Also at higher levels, the difference in temperature is small between CTRL, NoTMS and PBL Longtail, whereas the change in the vertical diffusion at higher levels has a large impact, giving a substantially stronger pole-equator temperature gradient in Longtail than in CTRL (this can be seen in Fig. 5 by using the thermal wind balance).

The annual mean near-surface wind speed is shown in Fig. 7. In CTRL, the spatial variability of wind speed is small over land. Over the continents, the wind speeds are generally higher in the three simulations without TMS. The differences are naturally largest over high topography regions. However, also in flatter regions, large areas display differences of 1–2 m s^{-1}, substantial numbers considering that the wind speeds over land generally lie between 0 and 2 m s^{-1} in CTRL. It is possible that the increased northwesterly advection over North America in NoTMS alleviates the warm bias in 2-m temperature that is seen in Fig. 6. Model discrepancies in the near-surface wind speed over sea are generally quite small for NoTMS–CTRL (Fig. 7b). There appears, however, to be a slight equatorward shift in the storm tracks in NoTMS and PBL Longtail at least in the Southern Hemisphere, where the maximum annual mean near surface zonal wind is found about 2 degrees further north than in CTRL (not shown). For Longtail (Fig. 7c), differences over sea are quite substantial in some regions. This is particularly true around the storm tracks, where the wind speeds appear to be higher in the Longtail simulation and display a clear poleward shift in both hemispheres.

3.1 Blocking

Blocks are quasi-stationary large-scale anticyclones that can block the flow and change the direction of traveling low pressure systems. As they can persist for several days

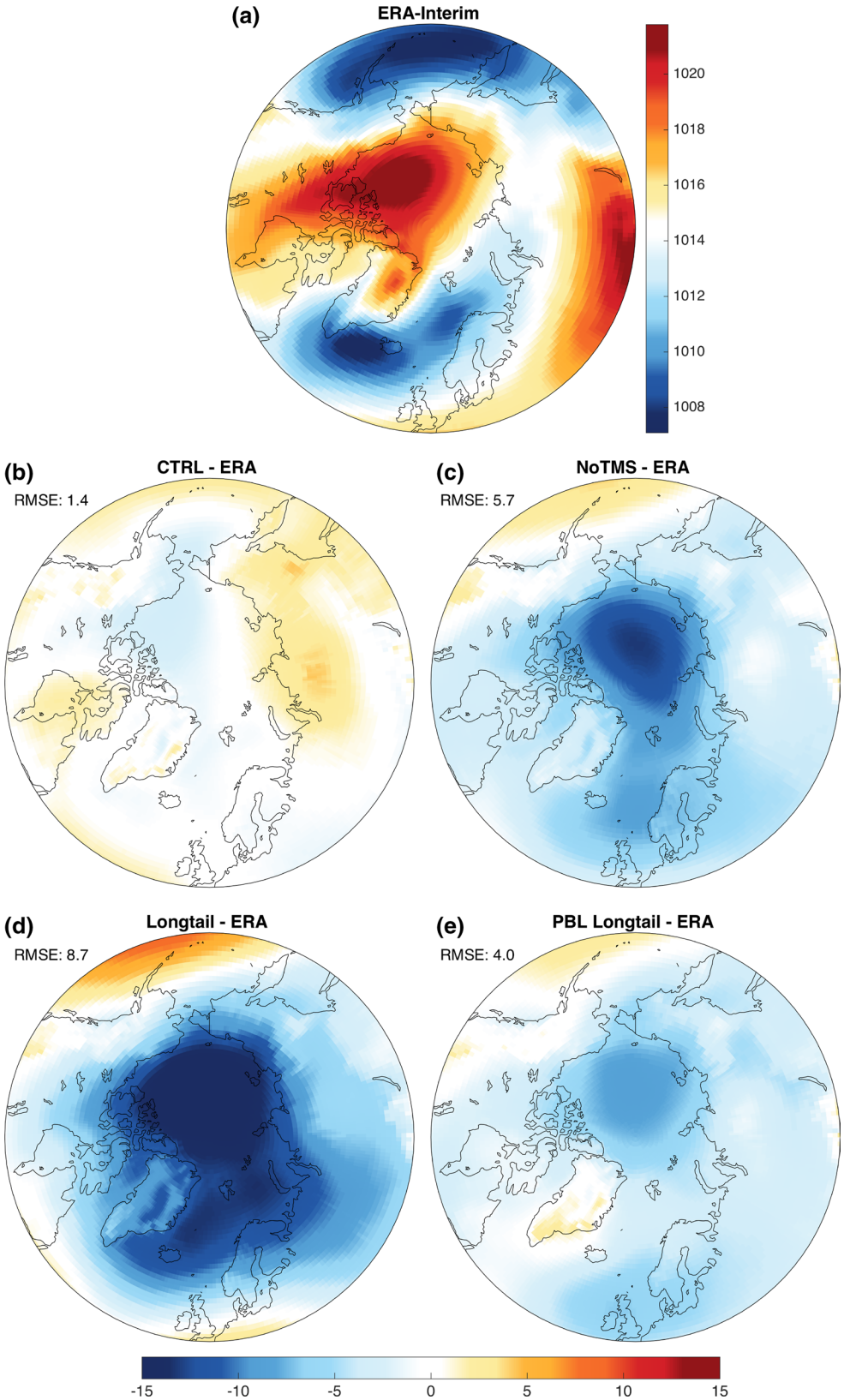

Fig. 3 The seasonal mean sea level pressure (hPa) for March–May over high latitudes at the Northern Hemisphere in **a** ERA-Interim, **b** CTRL–ERA-Interim, **c** NoTMS–ERA-Interim, **d** Longtail–ERA-Interim and **e** PBL Longtail–ERA-Interim. Also displayed is the area averaged RMSE for 50–90N

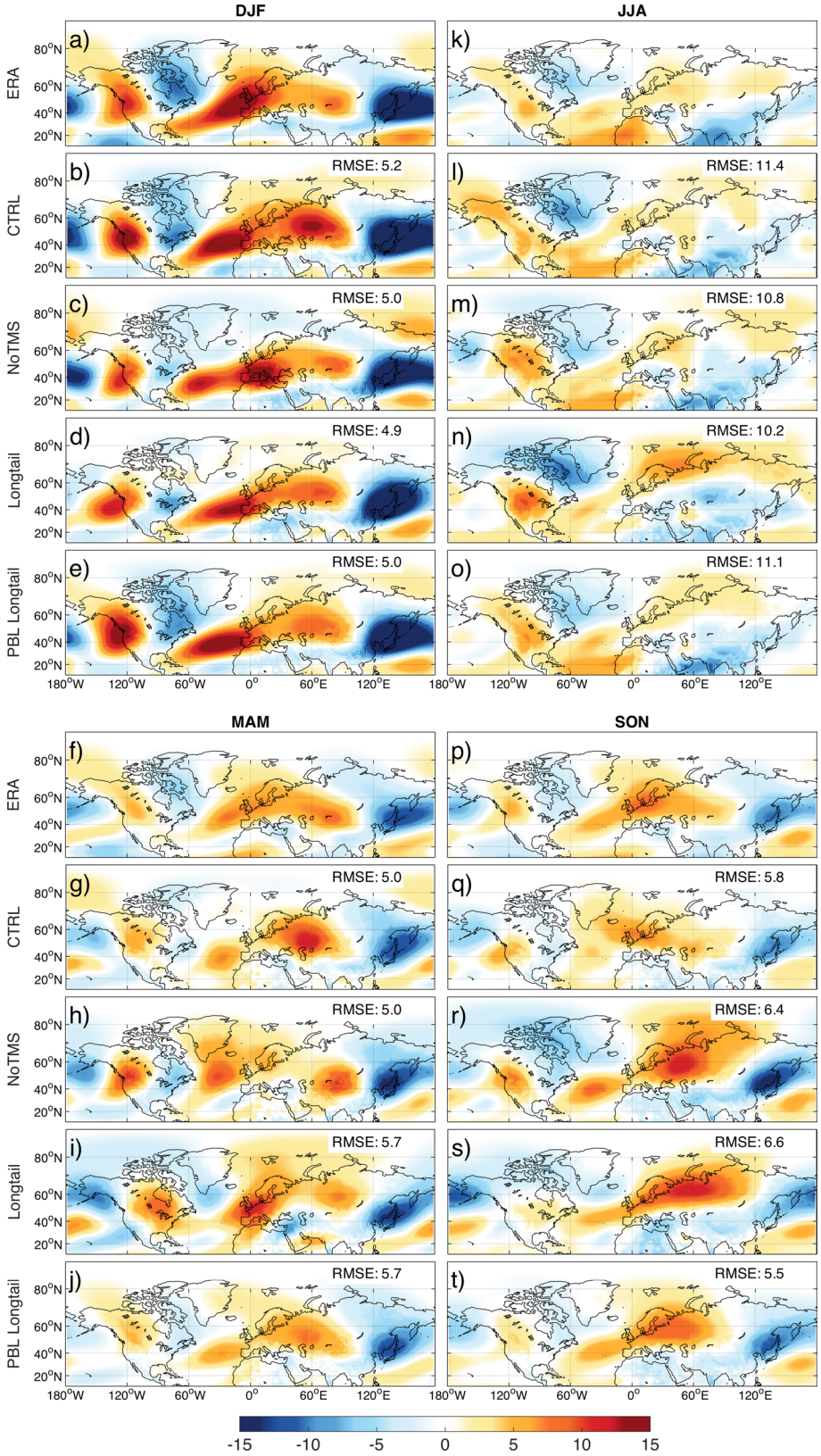

Fig. 4 The seasonal mean streamfunction anomaly at 500 hPa in the Northern Hemisphere. From *top* to *bottom* ERA-Interim, CTRL, NoTMS and Longtail for **a**–**e** December–February, **f**–**j** March–May, **k**–**o** June–August and **p**–**t** September–October. Also displayed is the area averaged RMSE for 10–90N

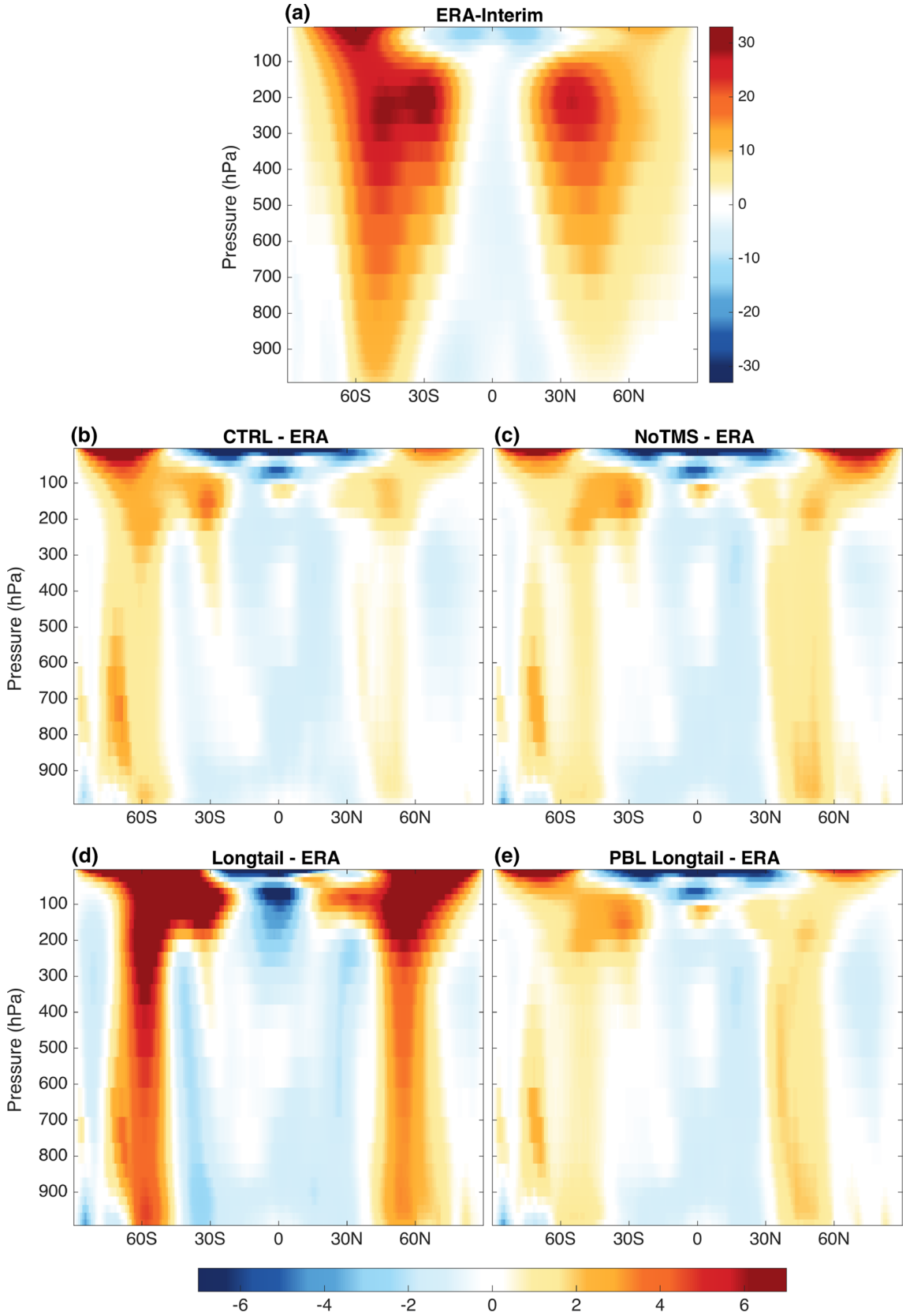

Fig. 5 The annual mean zonal mean wind. **a** ERA-Interim, **b** CTRL–ERA-Interim, **c** NoTMS–ERA-Interim, **d** Longtail–ERA-Interim and **e** PBL Longtail–ERA-Interim

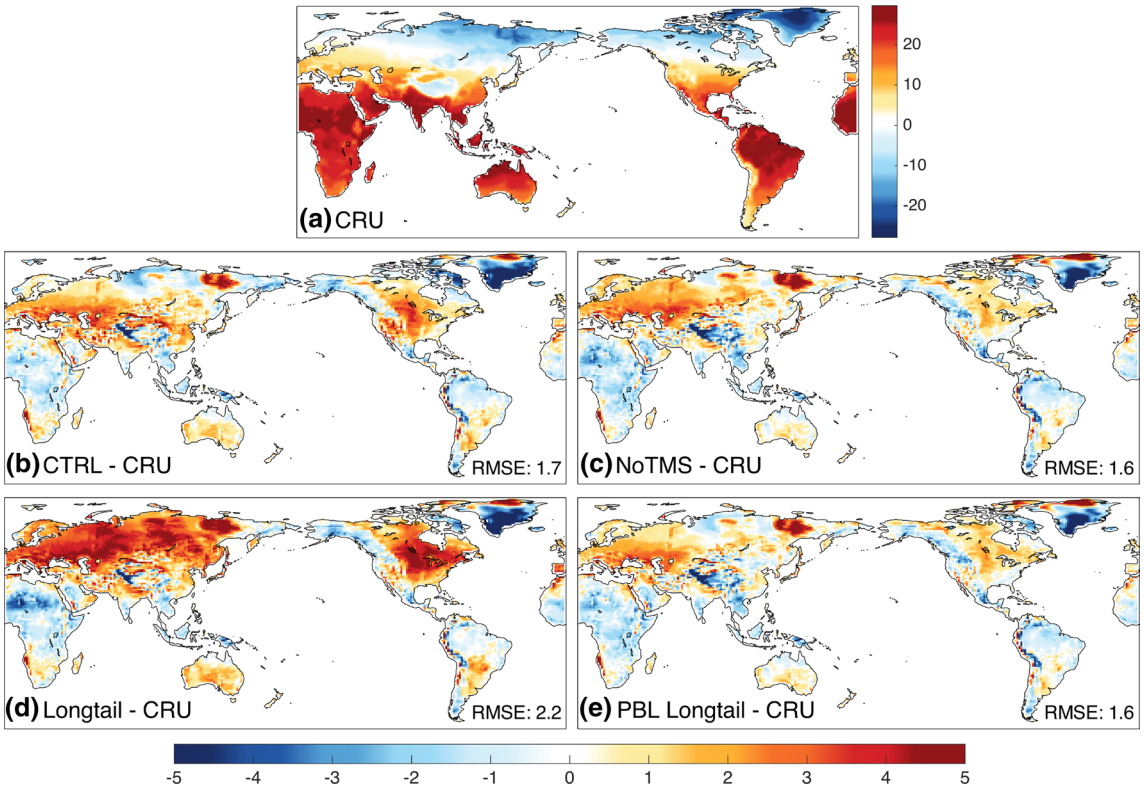

Fig. 6 Annual mean near surface temperature (°C) in **a** CRU and the difference between **b** CTRL–CRU, c) NoTMS–CRU, **d** Longtail–CRU and **e** PBL Longtail–CRU. RMSE is area averaged over all land areas except Antarctica

and up to weeks, their impact on the weather and climatology of a region is large. The frequency of atmospheric blocking tends to be underestimated by GCMs (Anstey et al. 2013; Masato et al. 2013; Dunn-Sigouin and Son 2013; D'Andrea et al. 1998). Figure 8 shows the annual and seasonal blocking frequencies in the Northern Hemisphere. The two reanalyses generally agree very well on the blocking frequency in all seasons, but with a slightly lower blocking episode frequency in MERRA, particularly over the Euro-Atlantic sector in fall.

Focusing first on the four main model simulations, CTRL, NoTMS, Longtail and PBL Longtail (thick, colored lines in Fig. 8), it can be seen that in the annual mean, all simulations severely underestimate the blocking frequency over the Euro-Atlantic region (Fig. 8a). CTRL is however slightly better than the rest and Longtail exhibits the poorest agreement with reanalyses. Over western Russia, the models, and especially CTRL, capture the blocking frequency rather well, whereas over the Pacific it is again underestimated, although less so in NoTMS.

The Atlantic blocking maximum (around 30°W–40°E) poses a problem for the models in all seasons, although winter seems to be the most problematic with far too few blockings in all simulations. However, during winter, the four main simulations are fairly similar, with only slightly more frequent blocking situations in NoTMS. In spring and autumn, there are larger model discrepancies and CTRL features more blockings and a much better agreement with the reanalyses than NoTMS and PBL Longtail over the Atlantic. Longtail has far too few blockings during all seasons, although in summer all three model simulations appears to better capture the blocking pattern over the Atlantic, Scandinavia and Russia.

The Pacific region (~100°E–240°E) paints a different picture. Here, the winter blockings are rather well captured by CTRL, NoTMS and PBL Longtail, whereas the other seasons show larger deviations between these simulations and the reanalyses. Longtail, however, substantially underestimate the frequency of blockings also in this region.

It appears as if the larger surface stress in CTRL increases and improves the simulated blocking frequency substantially over the Euro-Atlantic region (~60°W–60°E). It should be pointed out that the fact that we use climatological sea surface temperatures might affect the variability that could influence the simulated blocking frequency. However, the blocking pattern in NoTMS is similar to that in the previous version of the Community Atmosphere Model, CAM4 (Neale et al. 2013). It is therefore likely that the improvement in blocking frequency between CAM4 and CAM5 is largely due to the TMS parameterization. The

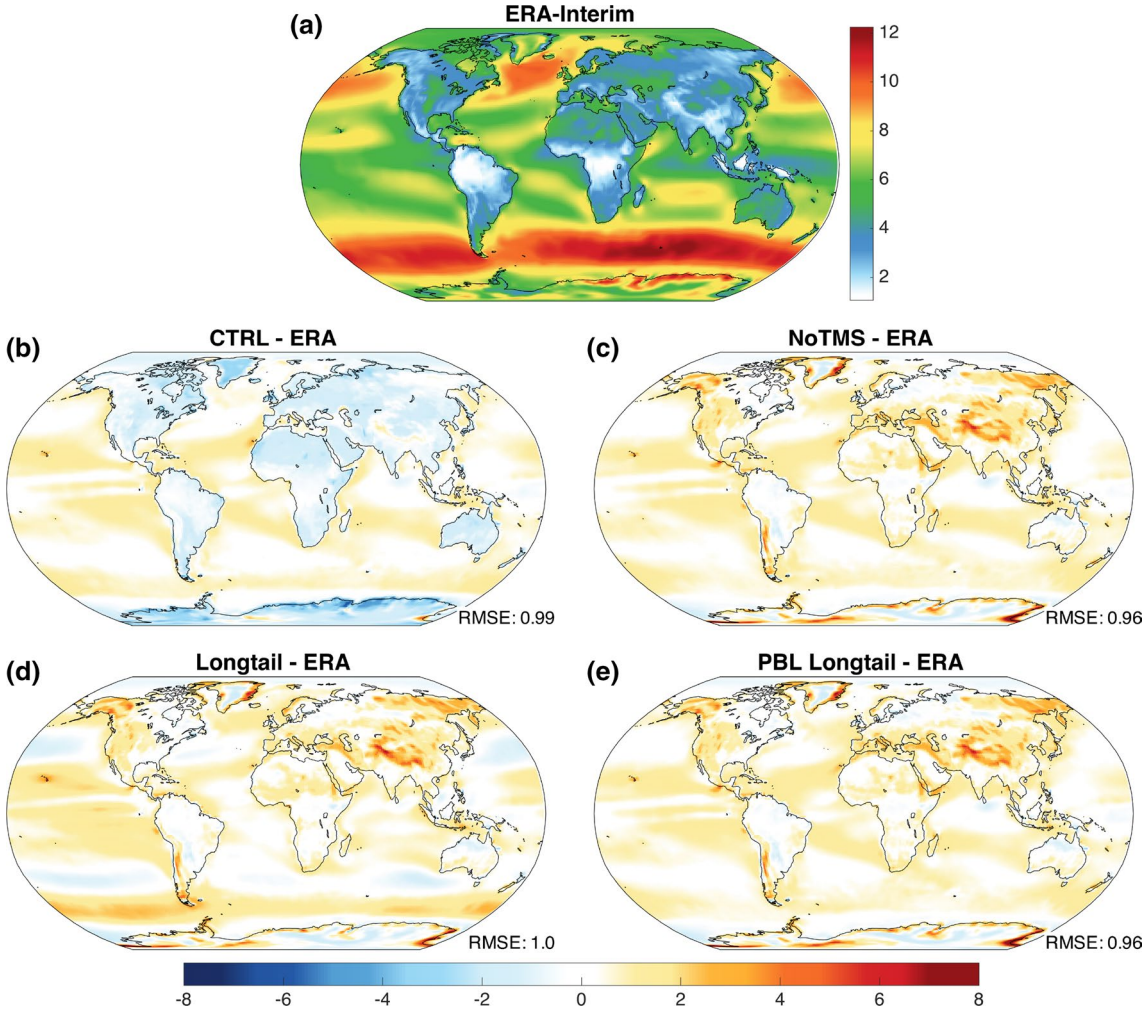

Fig. 7 Annual mean 10-m wind speed (m s^{-1}) in **a** ERA-Interim, **b** CTRL–ERA-Interim, **b** NoTMS–ERA-Interim, **c** Longtail–ERA-Interim and **d** PBL Longtail–ERA-Interim. RMSE is area averaged

underlying reasons remain unclear, but previous studies have pointed to the strength of the westerlies and the North Atlantic Oscillation as well as the position of the storm tracks as important for the blocking frequency (Zappa et al. 2014; Woollings et al. 2008; Barriopedro et al. 2006; Luo 2005), features that are all to some extent affected by TMS.

In order to examine possible causes for the observed impact of TMS on the blocking frequency, three more experiments are analyzed. TMS entails both a much larger turbulent drag over mountain regions and a substantial overall enhancement over the surface stress over land. To see if the large spatial differences in surface stress could be the main cause behind the better representation of blocking in CTRL, we perform a simulation called TMStopo. In this simulation, TMS is only applied in regions where the variation in the subgrid orography is large as these regions tend to coincide with regions with high topography (see Figure 4 in Lindvall et al. 2013). It is interesting that by only increasing the surface stress in these high-topography regions, the results are quite close to CTRL in spring over the Euro-Atlantic region (Fig. 8c). At the same time, the blocking frequency over the Pacific is enhanced (Fig. 8a). Also the blocking frequency in summer is improved compared to both CTRL and NoTMS and very close to the reanalyses (Fig. 8d). However, in winter when NoTMS and CTRL are very similar, TMStopo exhibits much larger biases over the Atlantic than both of them, while in autumn TMStopo is close to NoTMS (Fig. 8b, e). The basic state in TMStopo is, perhaps not so surprisingly, somewhere between CTRL and NoTMS, with for example the slightly stronger zonal winds and lower sea level pressure at high latitudes than in CTRL that is seen in NoTMS (not shown). However, the largest discrepancies from CTRL are found in spring and winter when the blocking frequency in TMStopo is either close to CTRL (spring) or deviates from both NoTMS and CTRL

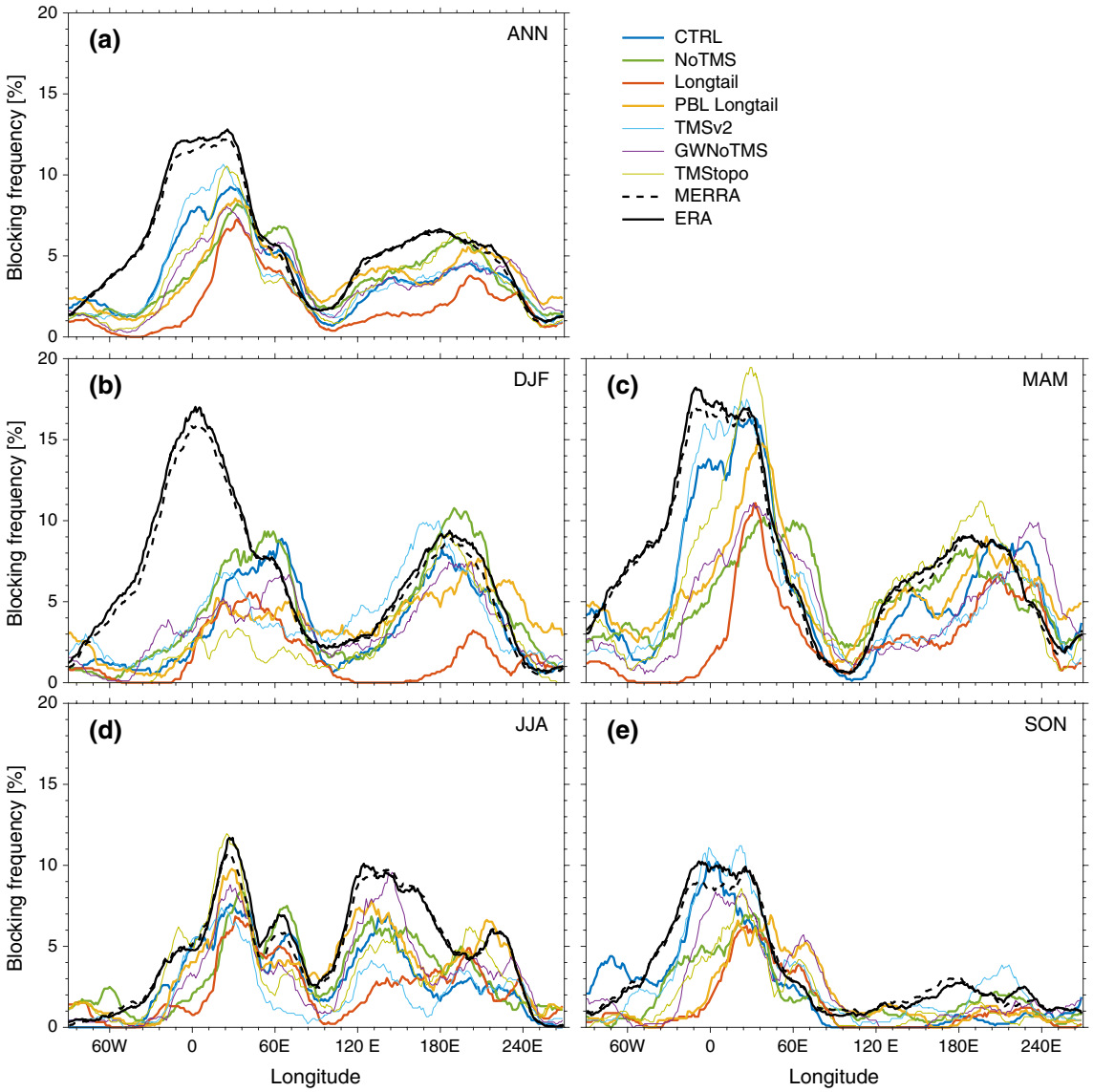

Fig. 8 Longitudinal distribution of Northern Hemisphere blocking frequency, where **a** shows the annual mean, **b** December–February, **c** March–May, **d** June–August and **e** September–November. *Black* indicates reanalyses, where ERA-Interim is represented by *solid lines* and MERRA by *dashed lines*. *Colored lines* represent the model simulations as denoted by the legend (see Table 1 for details on the simulations)

(winter). Summarizing, a large spatial difference in surface stress is favorable in summer but degrades the blocking pattern in winter and autumn. Thus, it seems as if the improvement in annual-mean blocking frequency due to TMS is to a large extent caused by the overall increase in surface drag over land.

One way in which the TMS parameterization in CTRL affects the general circulation and possibly blocking, is by the reduction of the low-level winds, which in turn reduces the gravity wave drag. The experiment GWNoTMS is similar to NoTMS, but the source winds in the gravity wave parameterization have been halved in order to only investigate the impact of the effect of reduced gravity wave drag. In the annual mean, GWNoTMS and CTRL appear to be almost identical over the Pacific (both with a lower blocking frequency than NoTMS and the reanalyses), but the agreement is less obvious in the separate seasonal plots. Over the Atlantic, the improvement compared to NoTMS is minor and most importantly, it does not lead to a substantial improvement in spring compared to NoTMS. The basic state of the atmosphere (zonal winds, sea level pressure and the 500 hPa geopotential height is in general similar in GWNoTMS and NoTMS. It cannot be ruled out that a too large gravity wave drag in NoTMS plays a role in the differences between CTRL and NoTMS, but it cannot explain all the differences seen.

By default, drag due to TMS is scaled by a factor dependent on the Richardson number, making TMS weaker in stably stratified conditions, turning it off completely when Ri > 1 (see Sect. 2). TMS appears to improve the simulation in spring to autumn over the Atlantic, but not in winter, when we expect a higher occurrence of stably stratified conditions. Therefore, a sixth experiment, TMSv2, was carried out with an unscaled TMS, that is, an enhanced surface stress for all stably stratified conditions. Although we do see an improvement in the annual mean compared to CTRL over the Atlantic, the effect is very small and mainly from the spring and autumn. In winter and also in summer, the simulation is actually degraded over western Russia. The basic state of the atmosphere in TMSv2 is generally close to CTRL. Strange enough, in winter, when the blocking frequency is degraded in TMSv2, the basic state seems to be even closer to ERA-interim than CTRL in terms of sea level pressure and 500 hPa geopotential height. So, although the mean state might cause some of the differences in blocking frequency, it is not the entire explanation.

3.2 Wind turning and cross-isobaric flow

The wind turning with height and the consequent ageostrophic flow in the boundary layer are important for the large-scale circulation and the development of synoptic cyclones (Adamson et al. 2006; Beare 2007; Svensson and Holtslag 2009). Figure 9 shows the distribution of the angle of the wind turning between the surface (in the soundings approximated with the 10 m height) and the top of the PBL at the ARM Southern Great Plains (SGP) site and Sodankylä in Northern Finland. Also included are the distributions of PBLH, wind speed at the surface and above the top of the PBL as well as the surface stress in the direction of the geostrophic wind. The boundary layer height is calculated using a bulk gradient Richardson number approach that follows Vogelezang and Holtslag (1996), which in turn is based on Troen and Mahrt (1986). The PBLH is determined iteratively by scanning upwards from the surface, until Ri exceeds the critical value of 0.3. The distributions in Fig. 9 are separated into different stability categories and the percentage of cases that falls into each category are indicated in the figure. The stability categories are defined using the flux Richardson number (Ri_f, Stull 1988) instead of the gradient Ri in order to minimize the impact of the difference in vertical resolution between models and observations. The flux Richardson number is defined as $Ri_f = \frac{-(g/\overline{\theta})\overline{\theta' w'}}{u_*^2 \partial \overline{U}/\partial z}$, The models capture the number of unstable cases fairly well at the ARM SGP site, but underestimate this number at the Sodankylä site (Fig. 9b) with 20 percentage points. Furthermore, both site have too many stable cases ($Ri_f > 0.02$, Fig. 9d) and too few weakly stable cases ($0 < Ri_f < 0.02$, Fig. 9c).

Fig. 9 The distribution of **a–d** the wind turning between the surface and the PBLH, **e–h** the PBLH, **i–l** the wind speed above the top of the PBL (*solid lines*, right axis) and at 10 m (*dashed lines*, left axis) and **m–p** $-\overline{u'w'_0}$, which can be seen as an estimate of the cross-isobaric flow (see Sect. 2 2.5 for further details). The distributions are shown for, in panels from left to right, all cases, unstably stratified cases (Ri < 0), weakly stably stratified cases (0 < Ri < 0.02) and stably stratified cases (Ri > 0.02). The percentages of cases in each stability class are given in the top panels. Distributions are calculated at midday and midnight local time

The NoTMS and PBL Longtail simulations agree well with the observations of wind turning at the ARM SGP site, whereas CTRL overestimates the turning of the wind (Fig. 9a–d). This is caused by the additional surface stress from the TMS parameterization included in CTRL that is too large at this flat grassland site with a small surface roughness. On the other hand, at the Sodankylä forest site, the simulations without TMS have a slightly negative bias in the wind turning, while all simulations have too little variation in the wind turning, with too sharp peaks in the distribution. This is particularly true for the stable cases. Also, the number of cases in the stable category are in all models about twice as many than what is observed (Fig. 9d). The wind turning in the Longtail simulation has too small wind turning angles for all stability categories at both places, but in particular in stable cases, where it retains stronger mixing than in the other three simulations. What is striking is that, the model results are so similar at the two locations, while the observations differ substantially. The Sodankylä gridbox, although dominated by forest, is rather mixed. But even comparing the results from a northern Finland grid box slightly further south with 90 % forest (not shown) and the ARM site grid box with over 80 % grassland, model wind turning is still very similar at the two completely different places.

The overall distribution of PBLH is very well represented by all simulations at both sites, except for CTRL at the ARM site (Fig. 9e). NoTMS, Longtail and PBL Longtail all capture the height of the PBL very well except for some problems with the weakly stable PBLs at the ARM site and the unstable PBLs at Sodankylä, where they have too many deep boundary layers. CTRL has the same problems and furthermore, also the stable boundary layers at the ARM site are too deep (Fig. 9e–h). It is possible that TMS gives too much surface stress at the flat ARM site, which has a negligible effect on the more turbulent, unstable PBLHs, but a stronger impact on the stable ones. When Ri is larger than one, however, TMS is turned off, which then might explain why the largest discrepancies are found in the weakly stable category. In Sodankylä, however, the effect of TMS is smaller as the vegetative roughness length is larger. The increased diffusion in the Longtail simulations seems to have a small impact on the PBLH as they are similar to NoTMS.

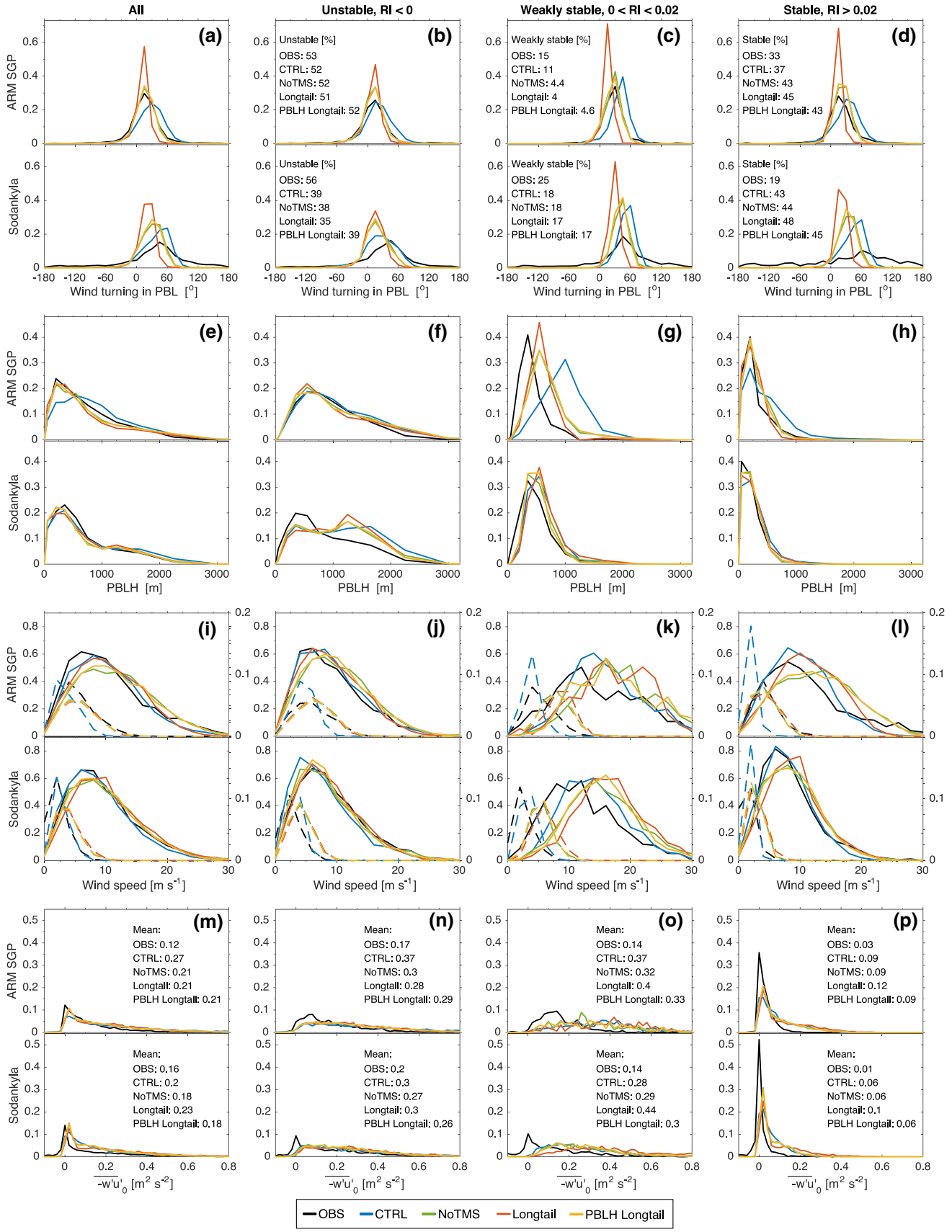
All
Unstable, RI < 0
Weakly stable, 0 < RI < 0.02
Stable, RI > 0.02
(a)
(b)
(c)
(d)
ARM SGP
Sodankyla
Unstable [%]
OBS: 53
CTRL: 52
NoTMS: 52
Longtail: 51
PBLH Longtail: 52
Unstable [%]
OBS: 56
CTRL: 39
NoTMS: 38
Longtail: 35
PBLH Longtail: 39
Weakly stable [%]
OBS: 15
CTRL: 11
NoTMS: 4.4
Longtail: 4
PBLH Longtail: 4.6
Weakly stable [%]
OBS: 25
CTRL: 18
NoTMS: 18
Longtail: 17
PBLH Longtail: 17
Stable [%]
OBS: 33
CTRL: 37
NoTMS: 43
Longtail: 45
PBLH Longtail: 43
Stable [%]
OBS: 19
CTRL: 43
NoTMS: 44
Longtail: 48
PBLH Longtail: 45
Wind turning in PBL [°]
(e)
(f)
(g)
(h)
PBLH [m]
(i)
(j)
(k)
(l)
Wind speed [m s-1]
(m)
(n)
(o)
(p)
Mean:
OBS: 0.12
CTRL: 0.27
NoTMS: 0.21
Longtail: 0.21
PBLH Longtail: 0.21
Mean:
OBS: 0.17
CTRL: 0.37
NoTMS: 0.3
Longtail: 0.28
PBLH Longtail: 0.29
Mean:
OBS: 0.14
CTRL: 0.37
NoTMS: 0.32
Longtail: 0.4
PBLH Longtail: 0.33
Mean:
OBS: 0.03
CTRL: 0.09
NoTMS: 0.09
Longtail: 0.12
PBLH Longtail: 0.09
Mean:
OBS: 0.16
CTRL: 0.2
NoTMS: 0.18
Longtail: 0.23
PBLH Longtail: 0.18
Mean:
OBS: 0.2
CTRL: 0.3
NoTMS: 0.27
Longtail: 0.3
PBLH Longtail: 0.26
Mean:
OBS: 0.14
CTRL: 0.28
NoTMS: 0.29
Longtail: 0.44
PBLH Longtail: 0.3
Mean:
OBS: 0.01
CTRL: 0.06
NoTMS: 0.06
Longtail: 0.1
PBLH Longtail: 0.06
-w'u'0 [m2 s-2]
OBS
CTRL
NoTMS
Longtail
PBLH Longtail

A similar pattern can be seen for the wind speeds (Fig. 9i–l). At the ARM site, the near-surface wind speeds (dashed lines) are to weak in CTRL, and although still slightly overestimated, the three simulations without TMS better represent them. However, at Sodankylä that has both forest and more orographic variations, CTRL is the one that agrees the best with observations. At the top of the PBL (solid lines), the differences between the model simulations are smaller, but here CTRL is generally closer to what is observed at both locations.

Figure 9m–p shows the surface stress in the opposite direction of the geostrophic wind. This stress can, as discussed in Sect. 22.5, be regarded as an estimate of the vertically integrated ageostrophic flow in the boundary layer. This estimate of the cross-isobaric flow is too large in all stability conditions, in all three simulations and at both sites. In unstable conditions, the wind-turning angle is larger in CTRL and the surface stress is also higher, resulting in a generally larger ageostrophic flow than in NoTMS and PBL Longtail. However, in weakly stable and stable conditions, the differences are smaller. The Longtail simulation has a similar and even slightly higher $-\overline{w'u'_0}$ in stable and weakly stable cases, which might also be due to the mixing in the free atmosphere and does not necessarily indicate a larger ageostrophic flow in the PBL.

It is clear that the large surface stress in CTRL gives larger wind turning angles, too large at the ARM site, but appropriate at Sodankylä. Previous studies have noted the opposite, that more diffusive turbulence closures with larger surface stress lead to smaller wind turning angles (e.g. Cuxart et al. 2006; Svensson and Holtslag 2009). We do see this in the Longtail simulation, but not in PBL Longtail, maybe due to the use of such a moderate longtail function. Svensson and Holtslag (2009) found that the enhanced diffusion gave deeper PBLs, which is not evident for the longtail simulations. Instead, only CTRL, with its large wind turning angles actually overestimates PBLH at the ARM site. Svensson and Holtslag (2009) also found that the vertically integrated ageostrophic flow was larger for the more diffusive turbulence closures. However, the increase of the surface stress in CTRL, most pronounced for unstable cases, and its deeper PBLs appear to make a bigger difference for the total cross-isobaric flow than the increase in diffusivity in PBL Longtail (Fig. 9m). It is interesting to note that although the additional surface stress appears to be beneficial for the large-scale flow, it seems to degrade the simulation of the wind turning and the ageostrophic flow in the boundary layer at the ARM site, but at the Sodankylä forest site the differences are smaller and CTRL is closer to the observations for several of the parameters.

4 Summary

Enhanced mixing is commonly used in NWP models and GCMs in order to reduce forecast errors and produce more realistic climate simulations. However, it is not supported by observations and tends to degrade simulations of the PBL. CAM5 does not use enhanced mixing and instead employs a subgrid-scale orographic drag parameterization, known as turbulent mountain stress (TMS), which increases the surface stress. This study has examined the sensitivity of the large-scale circulation in CAM5 to changes in the parameterizations of turbulence and orographic surface drag, using AMIP-type simulations. The CTRL simulation uses the default CAM5.3 physics, including TMS. CTRL is compared to NoTMS, a simulation without any subgrid-scale orographic surface stress. A comparison is also made with Longtail, a simulation without TMS but with a turbulence scheme that is more diffusive in stably stratified conditions, and with PBL Longtail, which only uses longtail stability functions in the PBL. Though, the longtail formulations that we include are quite modest compared to what is used in for example the IFS model employed by the ECMWF, their impact is still substantial.

From the analysis of these simulations we can conclude at the surface stress is very different in these four simulations. In CTRL, the contribution from TMS dominates completely over land. The large differences in surface stress causes substantial discrepancies in the near-surface winds, which are much lower over land in the CTRL simulation than in the simulations without TMS. Because the surface winds increase when TMS is turned off, there is a slight compensation from other drag parameterizations, leading to an enhancement of the gravity wave drag and the drag from turbulence. However, the resulting surface stress is still much larger in CTRL and in mountain regions, the annually-averaged magnitude of the surface stress can be up to one order of magnitude larger in CTRL than in NoTMS and the longtail simulations. Longtail has more diffusion in stably stratified conditions also at higher levels, which results in a larger surface stress in Longtail than in NoTMS, particularly in the storm track regions.

The differences in surface stress and vertical diffusion appears to impact the large-scale circulation of the atmosphere. One prominent feature is that the sea level pressure over the Arctic is substantially lower in NoTMS and even lower in Longtail than it is in CTRL, which agrees fairly well with ERA-Interim. Enhanced mixing in the PBL as in PBL Longtail, reduces the low pressure bias, but not as much as the improvement due to TMS. The enhanced mixing in PBL Longtail, is however, quite modest and it is possible that with even more diffusion in the PBL, the effect

would be similar to TMS. The zonal anomaly of the 500-hPa stream function also appears to be better represented in CTRL and PBL Longtail than in the other two simulations compared with ERA-Interim. The zonal mean zonal wind is too strong in all simulations and shifted poleward, but in the Northern Hemisphere, TMS reduces this bias substantially.

The representation of atmospheric blocking frequency is improved in CAM5 compared to CAM4. Blocking frequency is still generally underestimated in all simulations and seasons but particularly in winter over the Atlantic. However, the extra surface drag due to TMS appears to alleviate the transition-season biases seen in the NoTMS and longtail simulations. It therefore seems that the improvement between CAM4 and CAM5 is to a large extent due to the inclusion of TMS.

We can conclude that TMS leads to an improved simulation of the large-scale circulation in several respects, but the beneficial effects are not always apparent in the boundary layer flow. A comparison with observations from the Atmospheric Radiation Measurement (ARM) Southern Great Plains site in Oklahoma, US reveals that at this flat grassland site, the orographic surface stress in CTRL causes an excessively large reduction of the near-surface wind speeds. The wind turning in the PBL is also too strong, while the PBLH is overestimated. The surface stress in the direction opposite to the wind at the top of the boundary layer can be used as an estimate of the ageostrophic flow, which is important for the large-scale circulation and the development of synoptic cyclones. It is overestimated in all simulations, but in particular in CTRL.

On the other hand, at Sodankylä, a forest site with higher orography, the effect of TMS is still much smaller as the vegetative roughness length is larger. Here, the increase in surface stress in CTRL instead leads to a better agreement with observations when it comes to wind turning in the PBL and the magnitude of the near-surface wind speeds. The PBLHs and the cross-isobaric flow in the PBL are very similar in CTRL, NoTMS and PBL Longtail. At both sites, the effect of the very moderate enhancement of diffusion in the boundary layer in PBL Longtail does not have a large impact on the PBL, while the enhancement of diffusion throughout the atmospheric column gives a too small wind turning in the PBL. It should of course be noted that it is problematic to compare observations from a single observation site with a grid box representing a surface that is not completely homogeneous.

We can conclude that orographic surface stress and enhanced mixing in the PBL play similar roles in some respects for the large-scale circulation and climate, but while TMS greatly impacts both the large-scale circulation and the boundary layer, exchanging the short-tail stability functions for the modestly longer-tail ones only in the PBL has a smaller effect.

Acknowledgments We thank scientists at NCAR for enlightening discussions. We would like to acknowledge high-performance computing support from Yellowstone (ark:/85065/d7wd3xhc) provided by NCAR's Computational and Information Systems Laboratory, sponsored by the National Science Foundation. The CESM project is supported by the National Science Foundation and the Office of Science (BER) of the US Department of Energy.

References

Adamson DS, Belcher SE, Hoskins BJ, Plant RS (2006) Boundary-layer friction in midlatitude cyclones. Q J R Meteorol Soc 132(614):101–124. doi:10.1256/qj.04.145

Anstey JA (2013) Multi-model analysis of Northern Hemisphere winter blocking: model biases and the role of resolution. J Geophys Res Atmos 118(10):3956–3971. doi:10.1002/jgrd.50231

Barriopedro D, García-Herrera R, Lupo AR, Hernández E (2006) A climatology of Northern Hemisphere blocking. J Clim 19:1042–1063

Beare RJ (2007) Boundary layer mechanisms in extratropical cyclones. Q J R Meteorol Soc 133:503–515. doi:10.1002/qj.30

Beljaars AC, Brown AR, Wood N (2004) A new parametrization of turbulent orographic form drag. Q J R Meteorol Soc 130:1327–1347. doi:10.1256/qj.03.73

Bretherton CS, Park S (2009) A new moist turbulence parameterization in the Community Atmosphere Model. J Clim 22:3422–3448. doi:10.1175/2008JCLI2556.1

Brown AR, Beljaars ACM, Hersbach H, Hollingsworth A, Miller M, Vasiljevic D (2005) Wind turning across the marine atmospheric boundary layer. Q J R Meteorol Soc 131:1233–1250. doi:10.1256/qj.04.163

Brown AR, Beare RJ, Edwards JM, Lock AP, Keogh SJ, Milton SF, Walters DN (2008) Upgrades to the boundary-layer scheme in the Met Office numerical weather prediction model. Bound Layer Meteorol 128(1):117–132. doi:10.1007/s10546-008-9275-0

Chen G, Held IM, Robinson WA (2007) Sensitivity of the latitude of the surface westerlies to surface friction. J Atmos Sci 64(8):2899–2915. doi:10.1175/JAS3995.1

Cuxart J et al (2006) Single-column model intercomparison for a stably stratified atmospheric boundary layer. Bound Layer Meteorol 118:273–303. doi:10.1007/s10546-005-3780-1

D'Andrea F et al (1998) Northern Hemisphere atmospheric blocking as simulated by 15 atmospheric general circulation models in the period 1979–1988. Clim Dyn 14(6):385–407. doi:10.1007/s003820050230

Dunn-Sigouin E, Son S-W (2013) Northern Hemisphere blocking frequency and duration in the CMIP5 models. J Geophys Res Atmos 118:1179–1188. doi:10.1002/jgrd.50143

Fiedler F, Panofsky HA (1972) The geostrophic drag coefficient and the effective roughness length. Q J R Meteorol Soc 98(415):213–220. doi:10.1002/qj.49709841519

Fischer ML, Billesbach DP, Berry JA, Riley WJ, Torn MS (2007) Spatiotemporal variations in growing season exchanges of CO2, H2O, and sensible heat in agricultural fields of the Southern Great Plains. Earth Interact 11(17):1–21. doi:10.1175/EI231.1

Garratt JR (1992) The atmospheric boundary layer. Cambridge University Press, Cambridge 316 pp

Gregory D, Shutts GJ, Mitchell JR (1998) A new gravity-wave-drag scheme incorporating anisotropic orography and low-level wave breaking: impact upon the climate of the UK Meteorological Office Unified Model. Q J R Meteorol Soc 124:463–493

Holton JR, Hakim GJ (2012) An introduction to dynamic meteorology, 5th edn. Academic Press, Waltham 532 pp

Holtslag AAM et al (2013) Stable atmospheric boundary layers and diurnal cycles: challenges for weather and climate models. Bull Am Meteorol Soc 94(11):1691–1706. doi:10.1175/BAMS-D-11-00187.1

Hurrell JW, Hack JJ, Shea D, Caron JM, Rosinski J (2008) A new sea surface temperature and sea ice boundary dataset for the community atmosphere model. J Clim 21:5145–5153. doi:10.1175/2008JCLI2292.1

Hurrell JW et al (2013) The community earth system model: a framework for collaborative research. Bull Am Meteorol Soc 94:1339–1360. doi:10.1175/BAMS-D-12-00121.1

Kay JE et al (2012) Exposing global cloud biases in the Community Atmosphere Model (CAM) using satellite observations and their corresponding instrument simulators. J Clim 25(15):5190–5207. doi:10.1175/JCLI-D-11-00469.1

Lindvall J, Svensson G, Hannay C (2013) Evaluation of near-surface parameters in the two versions of the atmospheric model in CESM1 using flux station observations. J Clim 26(1):26–44. doi:10.1175/JCLI-D-12-00020.1

Lott F, Miller MJ (1997) A new subgrid-scale orographic drag parametrization: its formulation and testing. Q J R Meteorol Soc 123:101–127

Luo D (2005) Why is the North Atlantic block more frequent and long-lived during the negative NAO phase? Geophys Res Lett 32(20):L20Ã‚Â 804. doi:10.1029/2005GL022927

Mahrt L (1987) Grid-averaged surface fluxes. Mon Weather Rev 115:1550–1560

Masato G, Hoskins BJ, Woollings T (2013) Winter and summer Northern Hemisphere blocking in CMIP5 models. J Clim 26(18):7044–7059. doi:10.1175/JCLI-D-12-00466.1

Mauritsen T (2012) Advancing closures for stably stratified turbulence in global atmospheric models. In: Seminar proceedings of workshop on diurnal cycles and the stable boundary layer, 7–10, November 2011 ECMWF. Reading, England, pp 63–74

McCabe A, Brown AR (2007) The role of surface heterogeneity in modelling the stable boundary layer. Bound Layer Meteorol 122(3):517–534. doi:10.1007/s10546-006-9119-8

McFarlane NA (1987) The effect of orographically excited gravity wave drag on the general circulation of the lower stratosphere and troposphere. J Atmos Sci 44(14):1775–1800

Mitchell TD, Jones PD (2005) An improved method of constructing a database of monthly climate observations and associated high-resolution grids. Int J Climatol 25(6):693–712. doi:10.1002/joc.1181

Neale RB, Richter JH, Jochum M (2008) The impact of convection on ENSO: from a delayed oscillator to a series of events. J Clim 21(22):5904–5924. doi:10.1175/2008JCLI2244.1

Neale RB, Richter J, Park S, Lauritzen PH, Vavrus SJ, Rasch PJ, Zhang M (2013) The mean climate of the Community Atmosphere Model (CAM4) in forced SST and fully coupled experiments. J Clim 26(14):5150–5168. doi:10.1175/JCLI-D-12-00236.1

Neale RB et al (2010) Description of the NCAR Community Atmosphere Model (CAM 5.0). NCAR technical note TN-486

Palmer TN, Shutts GJ, Swinbank R (1986) Alleviation of a systematic westerly bias in general circulation and numerical weather prediction models through an orographic gravity wave drag parametrization. Q J R Meteorol Soc 112(474):1001–1039. doi:10.1002/qj.49711247406

Park S, Bretherton CS (2009) The University of Washington shallow convection and moist turbulence schemes and their impact on climate simulations with the Community Atmosphere Model. J Clim 22(12):3449–3469. doi:10.1175/2008JCLI2557.1

Richter JH, Rasch PJ (2008) Effects of convective momentum transport on the atmospheric circulation in the Community Atmosphere Model, version 3. J Clim 21(7):1487–1499. doi:10.1175/2007JCLI1789.1

Richter JH, Sassi F, Garcia RR (2010) Toward a physically based gravity wave source parameterization in a general circulation model. J Atmos Sci 67:136–156. doi:10.1175/2009JAS3112.1

Rienecker MM et al (2011) MERRA: NASAs modern-era retrospective analysis for research and applications. J Clim 24(14):3624–3648. doi:10.1175/JCLI-D-11-00015.1

Sandu I, Beljaars A, Bechtold P, Mauritsen T, Balsamo G (2013) Why is it so difficult to represent stably stratified conditions in numerical weather prediction (NWP) models? J Adv Model Earth Syst 5(2):117–133. doi:10.1002/jame.20013

Sandu I, Bechtold P, Beljaars A, Bozzo A, Pithan F, Shepherd TG, Zadra A (2016) Impacts of parameterized orographic drag on the Northern Hemisphere winter circulation. J Adv Model Earth Syst. doi:10.1002/2015MS000564

Simmons A, Uppala S, Dee D, Kobayashi S (2007) ERA-interim: new ECMWF reanalysis products from 1989 onwards. ECMWF Newsl 110:25–35

Stoffelen A, Anderson D (1997a) Scatterometer data interpretation: estimation and validation of the transfer function CMOD4. J Geophys Res 102(C3):5767–5780

Stoffelen A, Anderson D (1997b) Scatterometer data interpretation: measurement space and inversion. J Atmos Ocean Technol 14:1298–1313

Stull RB (1988) An introduction to boundary layer meteorology. Kluwer, Dordrecht 666 pp

Svensson G, Holtslag AAM (2009) Analysis of model results for the turning of the wind and related momentum fluxes in the stable boundary layer. Bound Layer Meteorol 132:261–277. doi:10.1007/s10546-009-9395-1

Tibaldi S, Molteni F (1990) On the operational predictability of blocking. Tellus 42A:343–365

Troen I, Mahrt L (1986) A simple model of the atmospheric boundary layer; sensitivity to surface evaporation. Bound Layer Meteorol 37:129–148

Viterbo P, Beljaars A, Mahfouf J-F, Teixeira J (1999) The representation of soil moisture freezing and its impact on the stable boundary layer. Q J R Meteorol Soc 125:2401–2426

Vogelezang DHP, Holtslag AAM (1996) Evaluation and model impacts of alternative boundary-layer height formulations. Bound Layer Meteorol 81:245–269. doi:10.1007/BF02430331

Woollings T, Hoskins B, Blackburn M, Berrisford P (2008) A new Rossby wave breaking interpretation of the North Atlantic Oscillation. J Atmos Sci 65(2):609–626. doi:10.1175/2007JAS2347.1

Xie S et al (2010) Clouds and more: ARM climate modeling best estimate data. Bull Am Meteorol Soc 91(1):13–20. doi:10.1175/2009BAMS2891.1

Zappa G, Masato G, Shaffrey L, Woollings T, Hodges K (2014) Linking Northern Hemisphere blocking and storm track biases in the CMIP5 climate models. Geophys Res Lett 41(1):135–139. doi:10.1002/2013GL058480

Zhang G, McFarlane N (1995) Sensitivity of climate simulations to the parameterization of cumulus convection in the Canadian Climate Centre general circulation model. Atmos Ocean 33(3):407–446

Zhao C et al (2013) A sensitivity study of radiative fluxes at the top of atmosphere to cloud-microphysics and aerosol parameters in the Community Atmosphere Model CAM5. Atmos Chem Phys 13(21):10Ã‚Â 969–10Ã‚Â 987. doi:10.5194/acp-13-10969-2013